Astron. Astrophys. 334, L5–L8 (1998)

ASTRONOMY AND ASTROPHYSICS

LETTER

Letter to the Editor

Variable sub-arcsecond structure in the circumstellar envelope of IRC+10216⋆

C.A. Haniff[1] **and D.F. Buscher**[2]

[1] Mullard Radio Astronomy Observatory, Cavendish Laboratory, Madingley Road, Cambridge CB3 0HE, UK (cah@mrao.cam.ac.uk)
[2] Department of Physics, University of Durham, South Road, Durham DH1 3LE, UK (david.buscher@durham.ac.uk)

Received 6 March 1998 / Accepted 7 April 1998

Abstract. We present new diffraction-limited interferometric images of the carbon star IRC+10216 at wavelengths of 2.2 μm and 3.4 μm. These show that the distribution of the near-infrared emission from the star departs significantly from a spherical geometry on 0.1 arcsecond scales. At 3.4 μm, i.e. close to the peak of the star/dust-shell spectral energy distribution, approximately 60% of the flux comes from regions asymmetrically disposed about the stellar photosphere at radii of 0.1-0.3 arcseconds. Images taken in 1989 and 1997 show large changes in the distribution of flux, but a consistent axis of symmetry at a PA of approximately -5 deg. Archival Hubble Space Telescope images at 0.79 and 1.06 μm show filaments with the same symmetry axis and a dark lane perpendicular to this axis approximately 0.25 arcseconds to the north of the star. Taken together, these data suggest a model in which the asymmetries seen are a consequence of envelope clearing along a bipolar axis. These observations indicate that the asymmetries seen in planetary nebulae may already be established before the progenitor star has left the AGB.

Key words: stars, AGB – stars, individual: IRC+10216 – stars, mass-loss

1. Introduction

As one of the brightest and closest carbon stars IRC+10216 (CW Leo, AFGL 1381) has been an ideal testing ground for models of the later phases of stellar evolution, which are important for our understanding of the formation of planetary nebulae and the chemical enrichment of the galaxy. Because the star is embedded in a dense dust shell whose inner radius cannot be resolved by conventional ground-based imaging, a favoured approach to the study of IRC+10216 has been via radiative-transfer modelling and spectral-energy distribution (SED) fitting (see, e.g. Griffin 1990, Ivezic & Elitzur 1996, Groenewegen 1997).

High resolution imaging of IRC+10216 has previously suggested the presence of asymmetric structure on small angular scales (see, e.g. Weigelt et al. (1997) for a recent H-band image), but essentially all radiative transfer models have assumed spherical symmetry for the dust shell. This is usually explained on two counts. First, since the asymmetries have typically been detected between 0.5 μm and 2.2 μm, i.e. at wavelengths shortward of the peak in the SED, it has been suggested that they might arise from scattering and contribute only insignificantly to the total bolometric flux from the dust shell. Second, it has been argued that the small-scale asymmetries may not be indicative of the long-term outflow from the star, as probed by molecular imaging (see, e.g. Groenewegen et al. 1997), and so may not be representative of the dominant structures in the dust shell.

In this letter we present new interferometric images of IRC+10216 obtained in 1989 and 1997 at wavelengths of 2.2 μm and 3.4 μm. The unprecedented spatial resolution of these data ($\sim 0.1''$) shows that in both wavebands the emission from the system is strongly asymmetric and is incompatible with a spherical model of radiatively heated dust. On the basis of our measurements, and archival HST images, we argue that a bipolar geometry for the overall dust distribution is favoured, and that minor modifications to spherical models to include a scattering component cannot explain the observations presented here.

2. Observations and data reduction

Observations of IRC+10216 were obtained at the Mayall 4-m telescope at Kitt Peak National Observatory, Tucson, on the nights of 1989 May 21 and 22, and at the United Kingdom Infrared Telescope on Mauna Kea, Hawaii, on 1997 March 29 and 30. In both cases sequences of several thousand short exposure images were secured using a 2-dimensional array detector through narrow-band filters centred on 2.2 μm and 3.4 μm. Similar observations were also made of a number of unresolved

Send offprint requests to: C.A. Haniff

⋆ Based, in part, on observations made with the NASA/ESA Hubble Space Telescope, obtained from the data archive at the Space Telescope Science Institute. STScI is operated by the Association of Universities for Research in Astronomy, Inc. under the NASA contract NAS 5-26555.

Table 1. Ground-based observation log

Dates	89/5/21,22	97/3/29,30
Telescope	KPNO 4 m	UKIRT 3.8 m
Image size (pixels)	62×58	128×128
Pixel size (arcseconds)	0.058	0.057
K bandpass (μm)[a]	2.22(0.09)	2.21(0.094)
L bandpass (μm)[a]	3.40(0.07)	3.41(0.072)
Seeing (arcseconds)[b]	1.1	0.6
Exposure time (ms)	50	36
Photometric phase	0.34	0.82

[a] Figures in parentheses are FWHM.
[b] Measured at 2.2 μm

reference stars and close binary systems to calibrate the instrumental transfer function and the orientation and pixel scales of the detectors. These were determined to 1° and 1% respectively. Details of the observations are given in Table 1.

Diffraction-limited maps of IRC+10216 were recovered from the short-exposure sequences using standard bispectral techniques. Following Haniff et al. (1989), the power-spectrum and bispectrum data were sampled so as to correspond to measurements taken with a multi-element VLBI array. After averaging, compensation for photon and readout noise biases, and calibration, the source visibilities and bispectrum (i.e. closure) phases were inverted using two independent radio astronomical mapping packages: the Caltech DIFMAP package (Shepherd 1997), which employs CLEAN to correct for the sparse *uv*-plane coverage, and an in-house Maximum Entropy-based self-calibration code (Sivia 1987). Apart from small differences attributable to enhanced resolution in the MEM reconstructions, both inversion strategies yielded identical images, confirming the reliability of the features reported here, and so we have only presented the MEM images in Fig. 1.

Calibrated narrowband images of IRC+10216 at $0.79\,\mu$m ($\Delta\lambda = 0.15\,\mu$m) and $1.06\,\mu$m ($\Delta\lambda = 0.13\,\mu$m) were also extracted from the HST data archive. The optical data were taken on 1996 October 20 with the Wide Field Planetary Camera at photometric phase 0.57, while the near-infrared measurements were made with the NICMOS instrument on 1997 April 30 (photometric phase $= 0.87$), i.e. very close to the same epoch as the UKIRT data presented here.

3. Results

Fig. 1 clearly demonstrates that there has been a considerable change in the morphology of the near-infrared emission from IRC+10216 and its surrounding dust shell in the past 8 years. Whereas in 1989 both the K and L-band emission were dominated by a single core, by 1997 there were four compact components, the brightest towards the south and the remainder (in order of decreasing brightness) in position angles 20°, -30°, and 65° at distances of $0.23''$, $0.21''$, and $0.20''$ from the brightest southern feature. Hereafter we shall refer to the brightest component

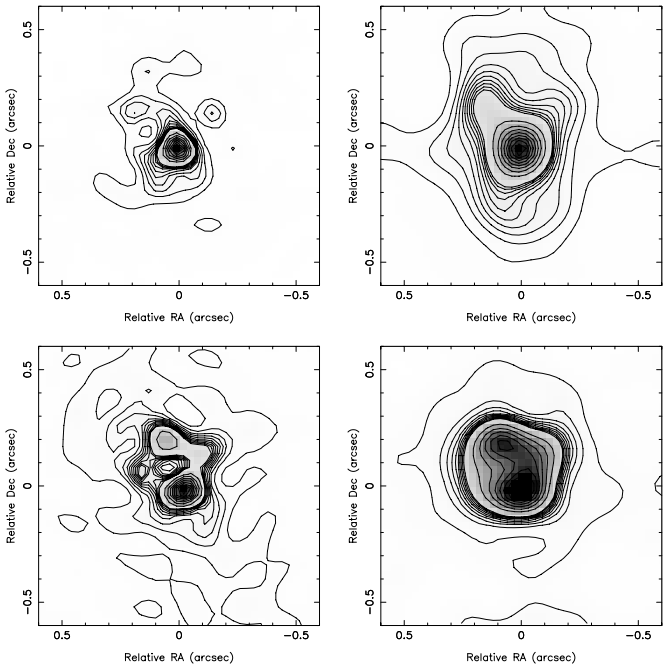

Fig. 1. Interferometric images of IRC+10216, obtained in narrow bands centred at K (left) and L (right), taken in 1989 May (top) and 1997 March (bottom). Contour levels are plotted at 1, 2, 3, 4, 5, 6, 7, 8, 9, 10, 20, 30, 40, 50, 60, 70, 80, and 90% of the peak. North is up and east to the left.

in each image as component A or the "core", measuring all position angles relative to it. We denote the other features in the 1997 images as components B (NNE), C (NNW), and D (NE). The spatial distribution of these features suggests the presence of a "hole" in the emission 0.1 arcsec NNE of the core. In 1989, rather than these additional compact features, the K and L-band images show diffuse lobes of emission to the NNE, to the SE, and to the NNW with an overall extent of $\pm 0.3''$.

Although the detailed structure of the dust-shell is quite different at the two epochs, our data reveal two long-lived axes. These are most clearly seen in the 1989 L-band image along approximate position angles of 30° and -40°, i.e. close to the directions of the vectors joining the core to components B and C in 1997. The variation in the near-infrared emission can thus be considered as one in which the relative strengths and locations of the compact components have changed with time. In 1989 these were all relatively weak, whereas by 1997 March they appear brighter and are seen clearly separated from the core. In particular, by this epoch component B had become very prominent, with peak brightnesses of approximately 30% and 60% of the core at $2.2\,\mu$m and $3.4\,\mu$m.

The infrared images from 1997 can be compared with HST data obtained at $0.79\,\mu$m in late 1996 and at $1.06\,\mu$m in mid-1997 (Fig. 2). Here the core is surrounded by a roughly elliptical halo of diffuse emission extending mainly to the SSW in the opposite direction to the majority of the extended infrared emission. At a level of 1% of the peak, the halo reaches approximately $1''$ from the core at both wavelengths, and at lower

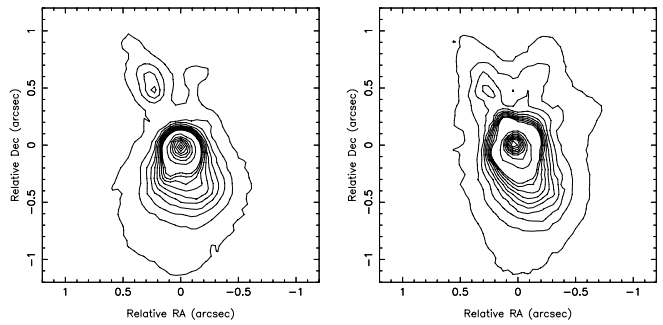

Fig. 2. HST images of IRC+10216 at wavelengths of 0.79μm (left) and 1.06μm (right). The data were secured in 1996 October and 1997 April respectively. Contour levels are plotted at 1, 2, 3, 4, 5, 6, 7, 8, 9, 10, 20, 30, 40, 50, 60, 70, 80, and 90% of the peak. North is up and east to the left.

levels fainter diffuse emission can be seen out to at least 2 arcseconds to the north and 3 arcseconds to the south. In the north the emission is concentrated into two narrow filaments that extend along PA's $\sim 25^\circ$ and $\sim -15^\circ$. The major differences between the $0.79\,\mu$m and $1.06\,\mu$m images relate to the disposition of the halo to the south. The nebulosity seen at $0.79\,\mu$m is quasi-reflection-symmetric about a line along PA 5°, and terminates abruptly to the north, presumably due to an increase in extinction, so that the filaments appear separated from the core by approximately $0.2''$. On the other hand, the halo seen at $1.06\,\mu$m shares an axis along PA $\sim 25^\circ$ with one of the filaments and exhibits a much more gradual decline in brightness to the north, consistent with reduced obscuration there.

4. Discussion

Because our interferometric reconstructions lack astrometric information, registration of the images, both between epochs and with the HST data, requires identification of at least one common feature in all the images. In the following paragraphs, we argue that the position of component A in the ground-based near-infrared maps can be identified as the position of the embedded star based on the relative fluxes and colours of the components, and that this identification of the core with the stellar position carries through to the HST images.

The images at $3.4\,\mu$m sample a wavelength close to the peak of the spectral energy distribution of the thermal emission from the hottest dust closest to the star, predicted to be at temperatures of 700-1000K and at distances of order $4R_*$ (Martin & Rogers 1987, Griffin 1990, Groenewegen et al. 1997). For an assumed distance of 150 pc, (Crosas & Menten 1997) this would correspond to an angular radius of approximately $0.08''$. At this wavelength, the scattering and absorption cross-sections of the dust are small compared to shorter wavelengths. As a result, the optical depth of the dust is expected to be relatively low (SED models typically predict that of order 10-15% of the total flux detected at these wavelengths comes directly from the stellar photosphere), and any flux not coming from the star would be expected to come preferentially from thermal emission from the dust nearest to the star, rather than coming from scattering by dust features at large radii from the star. Thus we expect the brightest emission at this wavelength to be concentrated within about 0.1 arcsec of the central star, and any dust seen at larger radii to be cooler and hence redder. This would lead us to identify component A as the emission from the star and the dust immediately around it, since it is both the brightest and the bluest component at this wavelength.

The core seen in the HST images can be identified with that seen in the ground-based observations because there is no evidence for any other compact component becoming more dominant at intermediate wavelengths. The $1.65\,\mu$m image from Weigelt et al. (1997) shows that the dominant features at this wavelength are the core and component B, $0.21''$ away in PA 20°. At $1.06\,\mu$m the presence of component B is revealed by the lobe visible in PA 20° at the lower contour levels. The registration between the cores of the HST images at $1.06\,\mu$m and $0.79\,\mu$m can be checked using the relative astrometry within each image: the distance between the brightest feature in the NE filament and the core differs by at most $0.05''$ in the two HST maps, an error of less than approximately one stellar diameter (Winters et al. 1995).

Having thus identified the core as being coincident with the star and its compact dust shell in each image, the gross changes in the extended emission longwards of $2.2\,\mu$m between 1989 and 1997 remain to be explained. The data from 1989 are consistent with a dominant spherically symmetric geometry, with minor contributions from diffuse asymmetric structures to the NNE, the SE, and the NNW. However, by 1997 only 22% of the L-band flux is contained within a circle of radius $0.1''$ centred on the core, and most of it (60%) appears as extended emission located between radii of 0.1 and 0.3 arcseconds. The K-L colour temperatures associated with these "inner" and "outer" zones are 620 K and 480 K respectively and thus consistent with thermal emission from dust at moderate distances from the star. It is possible that B and C are regions of enhanced dust density which were much closer to the star in 1989. If we assume a characteristic outflow velocity of $15\,\mathrm{kms}^{-1}$, typical of CO velocities in AGB stars, then over an 8-year period one would expect an angular displacement of $0.17''$, close to the separation of the core and these components. An alternative possibility is that the variations arise from changes in the heating of the dust during the star's photometric cycle: for example Ivezic & Elitzur (1996) predict an expansion of the inner dust condensation radius of 60% from minimum to maximum phase.

Overall, the combined optical and infrared data from 1997 clearly point towards a geometric model in which there is a dominant bipolar axis along PA 5° with an apparent half-opening angle of approximately 20°. This type of morphology has in the past been interpreted variously as evidence for:

1. A bipolar dust shell with an thick equatorial disk (Dyck et al. 1987)
2. A dust shell with an azimuthally symmetric density distribution varying in a smooth way above and below an equatorial plane (see, e.g. Collison & Fix 1991, Lopez et al. 1997)

3. A hybrid dust envelope resulting from the effects of an initial spherically symmetric AGB wind, and then an axially symmetric superwind phase of enhanced mass-loss in the equatorial plane (Meixner et al. 1997)
4. A spherical dust envelope with bipolar wind-blown holes (Whitney & Hartmann 1993, hereafter WH93)

The qualitative features of the data presented here favour the last of these possibilities. Within the framework of that model, the evacuated cavities are best seen via scattered emission at short wavelengths where the optical depth is high (WH93). This is consistent with Fig. 2 where the relative weakness of the northern lobe at $0.79\,\mu$m further implies a bipolar axis tilted towards the observer in the south: the foreground extinction from the surrounding unevacuated dust envelope attenuates the opposite lobe and enhances the visual prominence of the edges of the cavity, which are seen as the filaments in the HST images. A qualitiative comparison of the HST images and the models of WH93 suggest an inclination of order 20°. Note that this inclination is in the opposite sense to that proposed by Dyck et al. 1987, who interpreted the observed extended structure in their $2.2\,\mu$m one-dimensional speckle data as scattered emission from a bipolar halo obscured to the south by a thick equatorial disk.

At longer wavelengths the WH93 models predict a much more symmetric distribution of scattered flux, and so the asymmetries seen in the K and L bands must represent additional components of thermal emission. The location of all of these compact features towards the north is somewhat surprising, given the orientation of the bipolar flow described above, but interestingly components B, C, and D all lie at the edge of the band of enhanced extinction to the north of the core seen at optical wavelengths. One possible explanation, then, is that the knots of thermal emission seen at $2.2\,\mu$m and $3.4\,\mu$m are those clumps of dust within a toroidal structure in a plane perpendicular to the bipolar axis that happen to lie closest to the central star and thus appear hottest and brightest in these wavebands. The inclination of the torus would then allow a direct view of the star and its inner envelope while at the same time explaining the strong band of visual extinction running along PA 100° perpendicular to the bipolar axis. Alternatively, the brightest features might represent local density enhancements, or locations of additional heating via, for example, gas-dynamical processes.

However, whatever their origin, the measurements here provide strong evidence for a well-developed axisymmetric structure, enhanced opacity in a perpendicular plane, and variability on relatively short timescales. Whether this geometry has arisen through the "focussing" of an otherwise spherical flow by an equatorial torus, or through the clearing of a bipolar cavity by a fast wind remains unclear. It seems plausible that the asymmetries seen in IRC+10216 show structures which are the progenitors of the bipolar features often observed in the PPN (Meixner et al. 1997) and PN phases. Future observations will determine whether similar structures are commonplace at earlier evolutionary phases, and hopefully establish the epoch of their onset.

Acknowledgements. We are grateful to Debbie Pearson, Claire Chandler, and Andrew Marvell for valuable input, and to Julian Christou and Stephen Ridgway for assistance in securing the KPNO observations. CAH thanks the Royal Society for continued financial support.

References

Collison, A.J., Fix, J.D., 1991, ApJ 368, 545
Crosas, M., Menten, K.M., 1997, ApJ 483, 913
Dyck, H.M., Zuckerman, B., Howell, R.R., Beckwith, S., 1987, PASP, 99, 99
Griffin, I.P., 1990, MNRAS 247, 591
Groenewegen, M.A.T., 1997, A&A 317, 503
Groenewegen, M.A.T., van der Veen, W.E.C.J., Lefloch, B., Omont, A., 1997, A&A 322, L21
Haniff, C.A., Buscher, D.F., Christou, J.C., Ridgway, S.T., 1989, MNRAS 241, 51p
Ivezic, Z., Elitzur, M., 1996, MNRAS 279, 1019
Lopez, B., Tessier, E., Cruzalebes, P., Lefevre, J., Le Bertre, T., 1997, A&A, 322, 868
Martin, P.G., Rogers, C., 1987, ApJ 322, 374
Meixner, M., Skinner, C.J., Graham, J.R., Keto, E., Jernigan, J.G., Arens, J.F., 1997, ApJ 482, 897
Shepherd, M.C., 1997, Difmap: An Interactive Program for Synthesis Imaging. In: Astronomical Data Analysis Software and Systems VI, A.S.P. Conference Series, Hunt, G., Payne, H.E. (eds), Astronomical Society of the Pacific, vol. 125, 77
Sivia, D.S., 1987, PhD thesis, University of Cambridge
Weigelt, G., Balega, Y., Hofmann, K.-H., Langer, N., Osterbart, R., 1997, Interferometric studies of late phases of stellar evolution. In: Science with the VLTI, Paresce, F. (ed), Springer-Verlag, Berlin, p. 206
Whitney, B.A., Hartmann, L., ApJ, 402, 605 (WH93)
Winters, J.M., Fleischer, AJ, Gauger, A., Sedlmayr, E., 1995, A&A 302, 483